scientific reports

Check for updates

OPEN

Advanced fault location method for three-terminal distribution lines using frequency characteristics and μPMU data

Shuguang Li[1]✉, Houhe Chen[1], Changjiang Wang[1] & Xiaozhe Song[2]

The urban distribution network contains a significant number of multi- or three-terminal connections. Fault location in such networks is severely constrained by the lack of necessary conditions for deploying measuring instruments at intermediate connection points and the presence of erroneous or missing distribution line characteristics. This study designs a fault determination time index by analyzing the changes in Micro-phasor measurement unit (μPMU) measurement data at end nodes when an unbalanced fault occurs in the distribution line. A fault localization model incorporating frequency parameters is proposed, considering the influence of source load variations and the regular fluctuations of the fundamental frequency, which affect the characteristics of the distribution lines. To enhance the model's accuracy and efficiency, a solution approach combining Simulated Annealing Algorithm and trust region methods is suggested, addressing the impact of the initial values on the fault localization model calculation process. A three-terminal distribution line model is constructed in Matlab, and various failure scenarios are simulated. Using these frequency values significantly improved the accuracy of the fault location model's estimation results, achieving accuracy more than three times higher than models that do not consider frequency. The fault distance estimation error is reduced to less than 50 m. And, the model's applicable fault scenario is increased to 2000Ω. The results demonstrate that the proposed technique significantly improves the calculation efficiency and accuracy of the fault location model, providing a robust solution for fault location and line parameter estimation in distribution networks.

Keywords μPMU, Line parameter, Frequency, Simulate anneal arithmetic, Trust region

Fault diagnosis of distribution lines is a difficult problem facing the distribution network. Distribution line unbalanced faults(such as Single-line-to-ground faults, Line-to-line faults, and Double-line-to-ground faults) account for more than 50% of all faults in the distribution network[1–3]. The distribution network prioritizes the efficiency, precision, and cost-effectiveness of fault location methodologies, with a keen focus on rapid response times. Precise and prompt problem location lowers the operator's maintenance expenses and lessens the likelihood of worsening the issue.

Currently, transmission line fault location technology is the foundation for most distribution network fault location technologies[4–6]. The objective is to acquire voltage and current measurement data from distribution network nodes and lines, which is subsequently analyzed for fault characteristics to identify and locate faults within distribution lines, such as the traveling wave method[7–9], impedance method[10,11], state estimation[12], and machine learning[13–15]. The aforementioned methods have varying requirements for fault data, and all necessitate the deployment of measurement devices within distribution network nodes or lines. Then, measurement devices for distribution networks are mainly based on advanced metering infrastructure(AMI)[16], Smart Meters[17], Micro-phasor measurement unit (μPMU)[18–20], and other drives[21]. However, the wire-based location method, originally designed for extensive distribution network areas, is currently impractical. Despite this, the deployment of wire-based measuring devices across a substantial portion of the distribution network necessitates a reduction in associated costs. Balancing cost and accuracy, the integration of μPMUs with the aforementioned methods has garnered significant scholarly attention[22,23].

[1]School of Electrical Engineering, Northeast Electric Power University, Jilin 132012, China. [2]State Grid Jilin Electric Power Company Limited, Changchun 130022, China. ✉email: 20152617@neepu.edu.cn

The T-type lines (three-terminal and multi-terminal) vary in percentage within distribution networks based on specific regional factors, the age of the infrastructure, and the applicable design standards. These lines pose challenges in fault location, particularly due to insufficient measurement equipment in the public node segment[24–26]. In the context of three-terminal line fault localization or distribution line localization balancing, achieving an optimal balance between localization accuracy and solution cost can be addressed by leveraging low-cost μPMU information to achieve accurate fault localization.

Lin et al.[24] have cited several examples of this, including using synchronous measurement data and line parameters to construct fault location indicators, which can distinguish between faults within and outside the region in question, and subsequently calculate the distance to the fault. However, the accuracy of the required distribution line parameters may limit the applicability of this approach. Wang et al.[25] have deployed at the three-terminal node used voltage and current phase data, line parameters, and fault distance to construct the fault location equation and solved it using numerical optimization. This approach has been able to accurately calculate the fault distance but did not test the effect of frequency on the line operating parameters. In the field of electrical engineering, Yun et al.[26] have considered the measured voltage as line voltage and calculated the phase voltage phasor by using the line voltage phasor. Then, it used the measured data before and after the fault to construct the fault location equations, thereby improving the practical applicability of the method. To further reduce the dependence on measurement equipment, Panahi et al.[27] have considered the actual installation location and used the measurement data of two nodes to estimate the fault location of three-terminal lines. The aforementioned methodologies utilize the phase information of voltage and current, yet fail to consider the frequency information[28].

The distribution network is directly connected to the loads, and its frequency fluctuation is even more pronounced. With the advent of distributed energy sources, the frequency components of the distribution network will become more diverse[23]. Distribution lines are frequency-sensitive components, and thus, the effect of frequency must be taken into account during the calculation. Moreover, the dependence on the initial radius of the trust domain for faults occurring at different locations is not uniform. To address these issues, this paper proposes a fault location equation containing frequency based on reference[25] and introduces an index for determining the starting moment of the fault, which is established by a heuristic algorithm to provide the initial value for the calculation. This paper establishes the voltage and current operating equations of the three-terminal line in both the operational and fault states, based on the impedance model of the three-terminal distribution line. The main contributions are as follows:

1. It is important to establish a time reference for initiating the fault location process and to differentiate data before and after a fault occurs. By substituting the estimated voltage and current phase values from the μPMU into the operational process model, the point of fluctuation in the residuals of the equations can be identified. This point of fluctuation serves as the fault time reference.
2. The application of estimated frequency values as parameters in the line operation model capitalizes on the extensive data from μPMU to broaden the application scenarios of fault location models within distribution networks. The distribution network is influenced by fluctuations in source load, with the frequency of the network signal exhibiting a certain degree of variability. The distribution network signal contains a wealth of frequency information.
3. The integration of the simulated annealing algorithm with the trust domain enhances the solvability of the fault location calculation process. The occurrence of faults introduces uncertainty, which in turn affects the initial radius of the trust domain. Fault distances that are either too small or too large impede the solvability of the fault localization algorithm.

The paper is organized as follows: Sect. 2 introduces the distribution line frequency parameter model and analyzes the three-terminal line operation model under normal operation state and fault state. Section 3 introduces the proposed fault moment determination method and frequency-containing fault location model, and describes in detail the distribution line fault location fall solution method. Section 4 presents the localization results of the proposed method and those of existing methods in the same scenarios, and analyzes the localization results of the proposed method in different distribution line fault scenarios. Finally, the paper is summarized and an outlook is provided.

Distribution line model and frequency characteristic analysis

Line impedance is susceptible to changes in line operating frequency. This section is devoted to a detailed analysis of the frequency-dependent characteristics of line impedance, to develop the mathematical equations that describe the operation of T-lines in both normal and fault conditions.

Distribution line model frequency characteristic analysis

Since distribution network lines are shorter and have more branches than transmission network lines, which are longer and often adopt a dispersed architecture, the equivalent circuit utilized for analysis is typically the PI-type equivalent circuit. Figure 1. depicts the distribution lines, a comparable model.

The impact of the coupling parameters in the line is fully taken into account in Fig. 1. From a time-domain perspective, and the single-line-to-ground admittance has a negligible effect on the fluctuation of line current in the fault situations. Thus, Fig. 2. may be further simplified by ignoring the impact of the line-to-ground admittance during the fault-finding procedure.

According to Fig. 2., ignoring the effects of switching and environmental factors on the power distribution lines, it is assumed that the parameters of the three-phase power distribution lines are symmetrical, and the expression for three-phase impedance can be written as shown in Eq. (1)[29].

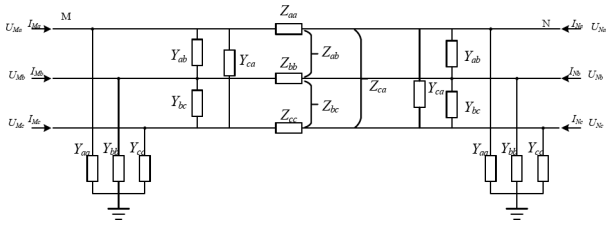

Fig. 1. The general model for distribution lines.

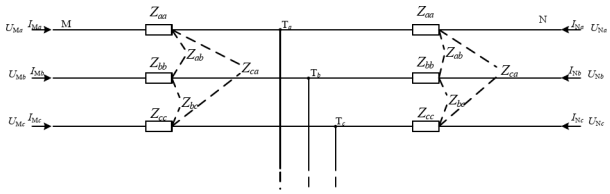

Fig. 2. The simplified equivalent model for distribution lines.

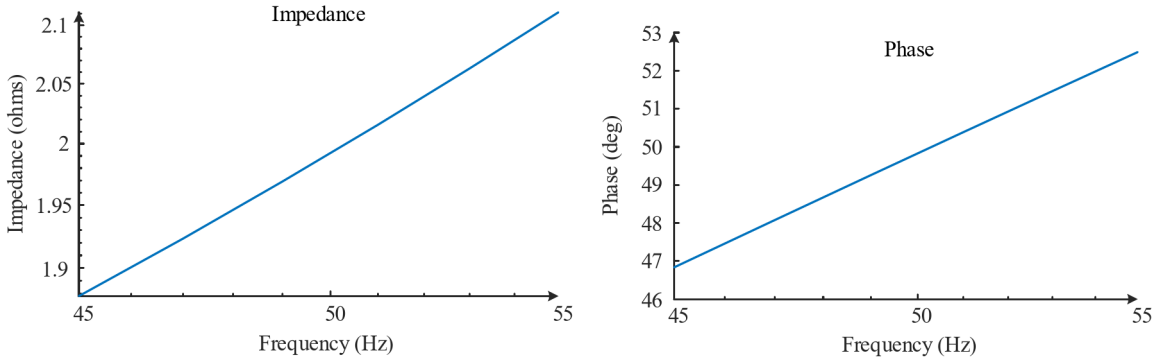

(a) Impedance change at different frequencies (b) Phase change at different frequencies

Fig. 3. Analysis of impedance frequency characteristics of the circuit.

$$Z_{ij} = D \times \begin{bmatrix} z_{\mathrm{SI}} & z_{\mathrm{MI}} & z_{\mathrm{MI}} \\ z_{\mathrm{MI}} & z_{\mathrm{SI}} & z_{\mathrm{MI}} \\ z_{\mathrm{MI}} & z_{\mathrm{MI}} & z_{\mathrm{SI}} \end{bmatrix} = D \times \begin{bmatrix} r_{\mathrm{SI}} + \mathrm{j}2\pi f \times l_{\mathrm{SI}} & r_{\mathrm{MI}} + \mathrm{j}2\pi f \times l_{\mathrm{MI}} & r_{\mathrm{MI}} + \mathrm{j}2\pi f \times l_{\mathrm{MI}} \\ r_{MI} + \mathrm{j}2\pi f \times l_{\mathrm{MI}} & r_{SI} + \mathrm{j}2\pi f \times l_{\mathrm{SI}} & r_{\mathrm{MI}} + \mathrm{j}2\pi f \times l_{\mathrm{MI}} \\ r_{MI} + \mathrm{j}2\pi f \times l_{\mathrm{MI}} & r_{MI} + \mathrm{j}2\pi f \times l_{\mathrm{MI}} & r_{\mathrm{SI}} + \mathrm{j}2\pi f \times l_{\mathrm{SI}} \end{bmatrix} \quad (1)$$

where D is the line length, $z_{\mathrm{SI}}$is the unit line self-impedance(SI), $z_{\mathrm{MI}}$is the unit line mutual impedance(MI), r_{SI} is the unit line self-resistance, l_{SI} is the unit line self-inductance, r_{MI} is the unit line mutual resistance, l_{SI} is the unit line mutual inductance, and f is the line's operating frequency, with obtained from the μPMU.

The distribution line is a frequency-sensitive element. Based on Eq. (1)., the impedance analysis of the circuit was constructed, and impedance and phase analysis of the circuit were carried out in the frequency range of 45–55 Hz, as shown in Fig. 3.

From Fig. 3, it may be seen that a variation in frequency will result in a corresponding change in the value of line impedance parameters. The operating frequency of the distribution network is not constant and is subject to fluctuations due to changes in distributed power sources, loads, and equipment operating states. The allowable fluctuation range for this frequency is 0.02 Hz. The μPMU may provide a more accurate value of the frequency, thus allowing for the introduction of frequency as a means of improving the accuracy of the line parameter estimation when the μPMU information is used for the impedance parameter estimation.

Distribution T-type model

The distribution network line wiring is available in various forms, with the T-type line being a more common type. This type of wiring does not allow for the installation of monitoring equipment at the intermediate nodes, and there is no new energy or load injection. Generally, at the three endpoints of the T-type line, monitoring equipment such as μPMU is installed, as shown in Fig. 4. Figure 4 illustrates the modified IEEE 14 node as an example. The nodes indicated as 2, 4, 3, and 8 represent the zero injection node, while the red, green, and yellow-labeled areas in the figure correspond to the typical T-type wiring.

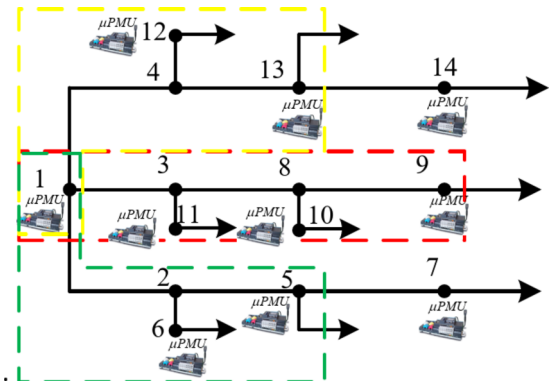

Fig. 4. Topology of the distribution network containing T-lines.

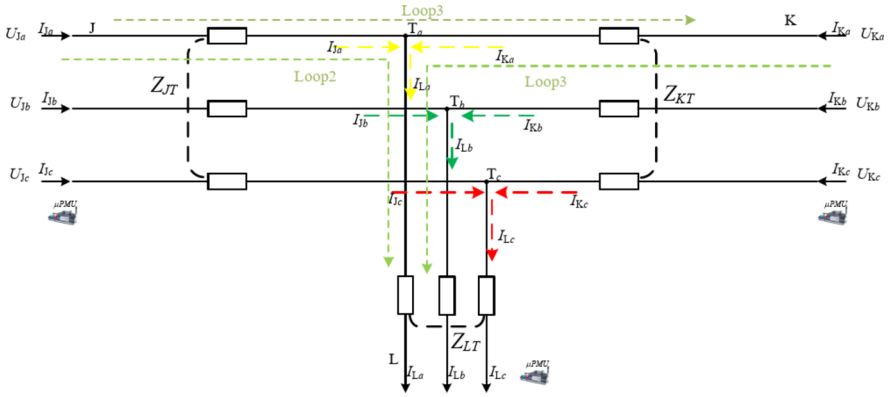

Fig. 5. Diagram of voltage and current analysis during normal operation of a T-type circuit.

To determine the voltage and current information under normal operating conditions, the T-type wiring is analyzed in conjunction with Fig. 5. Figure 5 shows the voltage and current flow of the three-phase system with nodes J, T, K, and L of T-type wiring.

To illustrate consider the c-phase of nodes J and K. The loop voltage equation is derived in accordance with Kirchhoff's law, as detailed in Eq. (2).

$$\dot{U}_{\mathrm{Jc}} - Z_{\mathrm{JTc\text{-}SI}} \times \dot{I}_{\mathrm{JTc}} - Z_{\mathrm{JTc\text{-}MI}} \times \dot{I}_{\mathrm{JTa}} - Z_{\mathrm{JTc\text{-}MI}} \times \dot{I}_{\mathrm{JTb}} = \dot{U}_{\mathrm{Kc}} - Z_{\mathrm{KTc}} \times \dot{I}_{\mathrm{KTc}} - Z_{\mathrm{KTc\text{-}MI}} \times \dot{I}_{\mathrm{KTa}} - Z_{\mathrm{KTc\text{-}MI}} \times \dot{I}_{\mathrm{KTb}} \quad (2)$$

where $\dot{U}_{\mathrm{Ka}}$is the voltage phasor of nodes J and K, $I_{\mathrm{JTa,b,c}}$, $I_{\mathrm{KTa,b,c}}$ is the current phasor of lines JT and KT.

The extension of Eq. (2) to the a, b, c phasor of nodes J and K is demonstrated in Eq. (3).

$$\begin{cases} \dot{U}_{\mathrm{Ja}} - Z_{\mathrm{JTa\text{-}SI}} \times \dot{I}_{\mathrm{JTa}} - Z_{\mathrm{JTa\text{-}MI}} \times \dot{I}_{\mathrm{JTb}} - Z_{\mathrm{JTa\text{-}MI}} \times \dot{I}_{\mathrm{JTc}} = \dot{U}_{\mathrm{Ka}} - Z_{\mathrm{KTa\text{-}SI}} \times \dot{I}_{\mathrm{KTa}} - Z_{\mathrm{KTa\text{-}MI}} \times \dot{I}_{\mathrm{KTb}} - Z_{\mathrm{KTa\text{-}MI}} \times \dot{I}_{\mathrm{KTc}} \\ \dot{U}_{\mathrm{Jb}} - Z_{\mathrm{JTb\text{-}SI}} \times \dot{I}_{\mathrm{JTb}} - Z_{\mathrm{JTb\text{-}MI}} \times \dot{I}_{\mathrm{JTa}} - Z_{\mathrm{JTb\text{-}MI}} \times \dot{I}_{\mathrm{JTc}} = \dot{U}_{\mathrm{Kb}} - Z_{\mathrm{KTb\text{-}SI}} \times \dot{I}_{\mathrm{KTb}} - Z_{\mathrm{KTb\text{-}MI}} \times \dot{I}_{\mathrm{KTa}} - Z_{\mathrm{KTb\text{-}MI}} \times \dot{I}_{\mathrm{KTc}} \\ \dot{U}_{\mathrm{Jc}} - Z_{\mathrm{JTc\text{-}SI}} \times \dot{I}_{\mathrm{JTc}} - Z_{\mathrm{JTc\text{-}MI}} \times \dot{I}_{\mathrm{JTa}} - Z_{\mathrm{JTc\text{-}MI}} \times \dot{I}_{\mathrm{JTb}} = \dot{U}_{\mathrm{Kc}} - Z_{\mathrm{KTc\text{-}SI}} \times \dot{I}_{\mathrm{KTc}} - Z_{\mathrm{KTc\text{-}MI}} \times \dot{I}_{\mathrm{KTa}} - Z_{\mathrm{KTc\text{-}MI}} \times \dot{I}_{\mathrm{KTb}} \end{cases} \quad (3)$$

The T-type line is capable of writing three loop voltage equations on the four nodes of the T-type line. According to Eq. (3), it is possible to write the voltage-current operating expression of the T-type line under normal operating conditions, as shown in Eq. (4).

$$\begin{cases} \dot{U}_{\mathrm{Ja}} - Z_{\mathrm{JTa\text{-}SI}} \times \dot{I}_{\mathrm{JTa}} - Z_{\mathrm{JTa\text{-}MI}} \times \dot{I}_{\mathrm{JTb}} - Z_{\mathrm{JTa\text{-}MI}} \times \dot{I}_{\mathrm{JTc}} = \dot{U}_{\mathrm{Ka}} - Z_{\mathrm{KTa\text{-}SI}} \times \dot{I}_{\mathrm{KTa}} - Z_{\mathrm{KTa\text{-}MI}} \times \dot{I}_{\mathrm{KTb}} - Z_{\mathrm{KTa\text{-}MI}} \times \dot{I}_{\mathrm{KTc}} \\ \dot{U}_{\mathrm{Jb}} - Z_{\mathrm{JTb\text{-}SI}} \times \dot{I}_{\mathrm{JTb}} - Z_{\mathrm{JTb\text{-}MI}} \times \dot{I}_{\mathrm{JTa}} - Z_{\mathrm{JTb\text{-}MI}} \times \dot{I}_{\mathrm{JTc}} = \dot{U}_{\mathrm{Kb}} - Z_{\mathrm{KTb\text{-}SI}} \times \dot{I}_{\mathrm{KTb}} - Z_{\mathrm{KTb\text{-}MI}} \times \dot{I}_{\mathrm{KTa}} - Z_{\mathrm{KTb\text{-}MI}} \times \dot{I}_{\mathrm{KTc}} \\ \dot{U}_{\mathrm{Jc}} - Z_{\mathrm{JTc\text{-}SI}} \times \dot{I}_{\mathrm{JTc}} - Z_{\mathrm{JTc\text{-}MI}} \times \dot{I}_{\mathrm{JTa}} - Z_{\mathrm{JTc\text{-}MI}} \times \dot{I}_{\mathrm{JTb}} = \dot{U}_{\mathrm{Kc}} - Z_{\mathrm{KTc\text{-}SI}} \times \dot{I}_{\mathrm{KTc}} - Z_{\mathrm{KTc\text{-}MI}} \times \dot{I}_{\mathrm{KTa}} - Z_{\mathrm{KTc\text{-}MI}} \times \dot{I}_{\mathrm{KTb}} \\ \dot{U}_{\mathrm{Ja}} - Z_{\mathrm{JTa\text{-}SI}} \times \dot{I}_{\mathrm{JTa}} - Z_{\mathrm{JTa\text{-}MI}} \times \dot{I}_{\mathrm{JTb}} - Z_{\mathrm{JTa\text{-}MI}} \times \dot{I}_{\mathrm{JTc}} = \dot{U}_{\mathrm{La}} - Z_{\mathrm{KTa\text{-}SI}} \times \dot{I}_{\mathrm{LTa}} - Z_{\mathrm{KTa\text{-}MI}} \times \dot{I}_{\mathrm{KTb}} - Z_{\mathrm{KTa\text{-}MI}} \times \dot{I}_{\mathrm{KTc}} \\ \dot{U}_{\mathrm{Jb}} - Z_{\mathrm{JTb\text{-}SI}} \times \dot{I}_{\mathrm{JTb}} - Z_{\mathrm{JTb\text{-}MI}} \times \dot{I}_{\mathrm{JTa}} - Z_{\mathrm{JTb\text{-}MI}} \times \dot{I}_{\mathrm{JTc}} = \dot{U}_{\mathrm{Lb}} - Z_{\mathrm{LTb\text{-}SI}} \times \dot{I}_{\mathrm{LTb}} - Z_{\mathrm{LTb\text{-}MI}} \times \dot{I}_{\mathrm{LTa}} - Z_{\mathrm{LTb\text{-}MI}} \times \dot{I}_{\mathrm{LTc}} \\ \dot{U}_{\mathrm{Jc}} - Z_{\mathrm{JTc\text{-}SI}} \times \dot{I}_{\mathrm{JTc}} - Z_{\mathrm{JTc\text{-}MI}} \times \dot{I}_{\mathrm{JTa}} - Z_{\mathrm{JTc\text{-}MI}} \times \dot{I}_{\mathrm{JTb}} = \dot{U}_{\mathrm{Lc}} - Z_{\mathrm{LTc\text{-}SI}} \times \dot{I}_{\mathrm{LTc}} - Z_{\mathrm{LTc\text{-}MI}} \times \dot{I}_{\mathrm{KTa}} - Z_{\mathrm{LTc\text{-}MI}} \times \dot{I}_{\mathrm{LTb}} \\ \dot{U}_{\mathrm{Ka}} - Z_{\mathrm{KTa\text{-}SI}} \times \dot{I}_{\mathrm{KTa}} - Z_{\mathrm{KTa\text{-}MI}} \times \dot{I}_{\mathrm{KTb}} - Z_{\mathrm{KTa\text{-}MI}} \times \dot{I}_{\mathrm{KTc}} = \dot{U}_{\mathrm{La}} - Z_{\mathrm{LTa\text{-}SI}} \times \dot{I}_{\mathrm{LTa}} - Z_{\mathrm{LTa\text{-}MI}} \times \dot{I}_{\mathrm{LTb}} - Z_{\mathrm{LTa\text{-}MI}} \times \dot{I}_{\mathrm{LTc}} \\ \dot{U}_{\mathrm{Kb}} - Z_{\mathrm{KTb\text{-}SI}} \times \dot{I}_{\mathrm{KTb}} - Z_{\mathrm{KTb\text{-}MI}} \times \dot{I}_{\mathrm{KTa}} - Z_{\mathrm{KTb\text{-}MI}} \times \dot{I}_{\mathrm{KTc}} = \dot{U}_{\mathrm{Lb}} - Z_{\mathrm{LTb\text{-}SI}} \times \dot{I}_{\mathrm{LTb}} - Z_{\mathrm{LTb\text{-}MI}} \times \dot{I}_{\mathrm{LTa}} - Z_{\mathrm{LTb\text{-}MI}} \times \dot{I}_{\mathrm{LTc}} \\ \dot{U}_{\mathrm{Kc}} - Z_{\mathrm{KTc\text{-}SI}} \times \dot{I}_{\mathrm{KTc}} - Z_{\mathrm{KTc\text{-}MI}} \times \dot{I}_{\mathrm{KTa}} - Z_{\mathrm{KTc\text{-}MI}} \times \dot{I}_{\mathrm{KTb}} = \dot{U}_{\mathrm{Lc}} - Z_{\mathrm{LTc\text{-}SI}} \times \dot{I}_{\mathrm{LTc}} - Z_{\mathrm{LTc\text{-}MI}} \times \dot{I}_{\mathrm{LTa}} - Z_{\mathrm{LTc\text{-}MI}} \times \dot{I}_{\mathrm{LTb}} \end{cases} \quad (4)$$

Equation (4) describes the relationship between the voltage and current at the three ends of the T-type line. If the distribution line parameters are accurate, the difference should be zero. Equation (4) can accurately describe the fluctuation of the T-type three-terminal voltage-current signal and the variation of line impedance.

Faulty operating state equations

Suppose a single earth fault occurs in phase c of line JT, and the distance of the fault from node J is d, as shown in Fig. 6:

At this point, the current flowing to the fault can be expressed according to KCL as:

$$\dot{I}_{fault} = \dot{I}_{\mathrm{JTc}} - \dot{I}'_{\mathrm{JTc}} = \dot{I}_{\mathrm{JTc}} - \left(\dot{I}_{\mathrm{LTc}} - \dot{I}_{\mathrm{KTc}}\right) \tag{5}$$

Based on Eq. (5), the voltage loop equation for phase C can be established as shown in Eq. (6):

$$\begin{cases} \dot{U}_{\mathrm{Jc}} - d \times z_{\mathrm{JTc\text{-}SI}} \times \dot{I}_{\mathrm{JTc}} - d \times z_{\mathrm{JTc\text{-}MI}} \times \dot{I}_{\mathrm{JTa}} - d \\ \times z_{\mathrm{JTc\text{-}MI}} \cdot \dot{I}_{\mathrm{JTb}} - (D_{\mathrm{LT}} - d) \times \left(z_{\mathrm{JTc\text{-}SI}} \times \left(\dot{I}_{\mathrm{LTc}} - \dot{I}_{\mathrm{KTc}}\right)\right) \\ - (D_{\mathrm{LT}} - d) \times \left(z_{\mathrm{JTc\text{-}MI}} \cdot \left(\dot{I}_{\mathrm{LTa}} - \dot{I}_{\mathrm{KTa}}\right)\right) \\ - (D_{\mathrm{LT}} - d) \times \left(z_{\mathrm{JTc\text{-}MI}} \times \left(\dot{I}_{\mathrm{LTb}} - \dot{I}_{\mathrm{KTb}}\right)\right) = \dot{U}_{\mathrm{Kc}} - D_{\mathrm{KT}} \times z_{\mathrm{KTc\text{-}SI}} \\ \times \dot{I}_{\mathrm{KTc}} - D_{\mathrm{KT}} \times z_{\mathrm{KTc\text{-}MI}} \times \dot{I}_{\mathrm{KTa}} - D_{\mathrm{KT}} \\ \times z_{\mathrm{KTc\text{-}MI}} \times \dot{I}_{\mathrm{KTb}} \end{cases} \tag{6}$$

Where d is the fault distance.

Introducing the fault distance in Eq. (6), the fault distance can be calculated by simply substituting the voltage and current data measured by the μPMU and the line parameters into the equation. In practice, the error of the calculated fault distance is large due to the large deviation between the actual and nominal values of the distribution line parameters. If the line parameters are taken as unknown quantities, the number of equations needs to be further supplemented.

Design of T-line fault localization model based on μPMU

The distribution line fault location model can be divided into two parts: the first part of fault location initiation and the second part of fault location calculation. The fault location initiation phase focuses on determining the start time of the fault, and the measurement data required for fault location calculation provides a time base.

Fault location time start judgment

Equation (4) is further analyzed when the resistance and inductance values of the distribution network line are constant. Theoretically, the two ends of Eq. equals should be equal. When a fault occurs on the line, the estimated value of the micro PMU fluctuates due to the influence of voltage and current signal fluctuations, and a deviation occurs at both ends of the equation. Using this deviation as an activation criterion, changes in the line will be acutely detected. For this purpose, the distribution line operation model under normal state is established:

$$\begin{cases} g(1) = \dot{U}_{\mathrm{Ja}} - Z_{\mathrm{JTa\text{-}SI}} \times \dot{I}_{\mathrm{JTa}} - Z_{\mathrm{JTa\text{-}MI}} \times \dot{I}_{\mathrm{JTb}} - Z_{\mathrm{JTa\text{-}MI}} \times \dot{I}_{\mathrm{JTc}} - \dot{U}_{\mathrm{Ka}} + Z_{\mathrm{KTa\text{-}SI}} \times \dot{I}_{\mathrm{KTa}} + Z_{\mathrm{KTa\text{-}MI}} \times \dot{I}_{\mathrm{KTb}} + Z_{\mathrm{KTa\text{-}MI}} \times \dot{I}_{\mathrm{KTc}} = 0 \\ g(2) = \dot{U}_{\mathrm{Jb}} - Z_{\mathrm{JTb\text{-}SI}} \times \dot{I}_{\mathrm{JTb}} - Z_{\mathrm{JTb\text{-}MI}} \times \dot{I}_{\mathrm{JTa}} - Z_{\mathrm{JTb\text{-}MI}} \times \dot{I}_{\mathrm{JTc}} - \dot{U}_{\mathrm{Kb}} + Z_{\mathrm{KTb\text{-}SI}} \times \dot{I}_{\mathrm{KTb}} + Z_{\mathrm{KTb\text{-}MI}} \times \dot{I}_{\mathrm{KTa}} + Z_{\mathrm{KTb\text{-}MI}} \times \dot{I}_{\mathrm{KTc}} = 0 \\ g(3) = \dot{U}_{\mathrm{Jc}} - Z_{\mathrm{JTc\text{-}SI}} \times \dot{I}_{\mathrm{JTc}} - Z_{\mathrm{JTc\text{-}MI}} \times \dot{I}_{\mathrm{JTa}} - Z_{\mathrm{JTc\text{-}MI}} \times \dot{I}_{\mathrm{JTb}} - \dot{U}_{\mathrm{Kc}} + Z_{\mathrm{KTc\text{-}SI}} \times \dot{I}_{\mathrm{KTc}} + Z_{\mathrm{KTc\text{-}MI}} \times \dot{I}_{\mathrm{KTa}} + Z_{\mathrm{KTc\text{-}MI}} \times \dot{I}_{\mathrm{KTb}} = 0 \\ g(4) = \dot{U}_{\mathrm{Ja}} - Z_{\mathrm{JTa\text{-}SI}} \times \dot{I}_{\mathrm{JTa}} - Z_{\mathrm{JTa\text{-}MI}} \times \dot{I}_{\mathrm{JTb}} - Z_{\mathrm{JTa\text{-}MI}} \times \dot{I}_{\mathrm{JTc}} - \dot{U}_{\mathrm{La}} + Z_{\mathrm{KTa\text{-}SI}} \times \dot{I}_{\mathrm{LTa}} + Z_{\mathrm{KTa\text{-}MI}} \times \dot{I}_{\mathrm{KTb}} + Z_{\mathrm{KTa\text{-}MI}} \times \dot{I}_{\mathrm{KTc}} = 0 \\ g(5) = \dot{U}_{\mathrm{Jb}} - Z_{\mathrm{JTb\text{-}SI}} \times \dot{I}_{\mathrm{JTb}} - Z_{\mathrm{JTb\text{-}MI}} \times \dot{I}_{\mathrm{JTa}} - Z_{\mathrm{JTb\text{-}MI}} \times \dot{I}_{\mathrm{JTc}} - \dot{U}_{\mathrm{Lb}} + Z_{\mathrm{LTb\text{-}SI}} \times \dot{I}_{\mathrm{LTb}} + Z_{\mathrm{LTb\text{-}MI}} \times \dot{I}_{\mathrm{LTa}} + Z_{\mathrm{LTb\text{-}MI}} \times \dot{I}_{\mathrm{LTc}} = 0 \\ g(6) = \dot{U}_{\mathrm{Jc}} - Z_{\mathrm{JTc\text{-}SI}} \times \dot{I}_{\mathrm{JTc}} - Z_{\mathrm{JTc\text{-}MI}} \times \dot{I}_{\mathrm{JTa}} - Z_{\mathrm{JTc\text{-}MI}} \times \dot{I}_{\mathrm{JTb}} - \dot{U}_{\mathrm{Lc}} + Z_{\mathrm{LTc\text{-}SI}} \times \dot{I}_{\mathrm{LTc}} + Z_{\mathrm{LTc\text{-}MI}} \times \dot{I}_{\mathrm{KTa}} + Z_{\mathrm{LTc\text{-}MI}} \times \dot{I}_{\mathrm{LTb}} = 0 \\ g(7) = \dot{U}_{\mathrm{Ka}} - Z_{\mathrm{KTa\text{-}SI}} \times \dot{I}_{\mathrm{KTa}} - Z_{\mathrm{KTa\text{-}MI}} \times \dot{I}_{\mathrm{KTb}} - Z_{\mathrm{KTa\text{-}MI}} \times \dot{I}_{\mathrm{KTc}} - \dot{U}_{\mathrm{La}} + Z_{\mathrm{LTa\text{-}SI}} \times \dot{I}_{\mathrm{LTa}} + Z_{\mathrm{LTa\text{-}MI}} \times \dot{I}_{\mathrm{LTb}} + Z_{\mathrm{LTa\text{-}MI}} \times \dot{I}_{\mathrm{LTc}} = 0 \\ g(8) = \dot{U}_{\mathrm{Kb}} - Z_{\mathrm{KTb\text{-}SI}} \times \dot{I}_{\mathrm{KTb}} - Z_{\mathrm{KTb\text{-}MI}} \times \dot{I}_{\mathrm{KTa}} - Z_{\mathrm{KTb\text{-}MI}} \times \dot{I}_{\mathrm{KTc}} - \dot{U}_{\mathrm{Lb}} + Z_{\mathrm{LTb\text{-}SI}} \times \dot{I}_{\mathrm{LTb}} + Z_{\mathrm{LTb\text{-}MI}} \times \dot{I}_{\mathrm{LTa}} + Z_{\mathrm{LTb\text{-}MI}} \times \dot{I}_{\mathrm{LTc}} = 0 \\ g(9) = \dot{U}_{\mathrm{Kc}} - Z_{\mathrm{KTc\text{-}SI}} \times \dot{I}_{\mathrm{KTc}} - Z_{\mathrm{KTc\text{-}MI}} \times \dot{I}_{\mathrm{KTa}} - Z_{\mathrm{KTc\text{-}MI}} \times \dot{I}_{\mathrm{KTb}} - \dot{U}_{\mathrm{Lc}} + Z_{\mathrm{LTc\text{-}SI}} \times \dot{I}_{\mathrm{LTc}} + Z_{\mathrm{LTc\text{-}MI}} \times \dot{I}_{\mathrm{LTa}} + Z_{\mathrm{LTc\text{-}MI}} \times \dot{I}_{\mathrm{LTb}} = 0 \end{cases} \tag{7}$$

Equation (7) involves complex number operations that consume a lot of computing time and to require further organization of Eq. (7) to make the real and imaginary parts of the equation equal to zero. This turns Eq. (7) into 18 Eq.

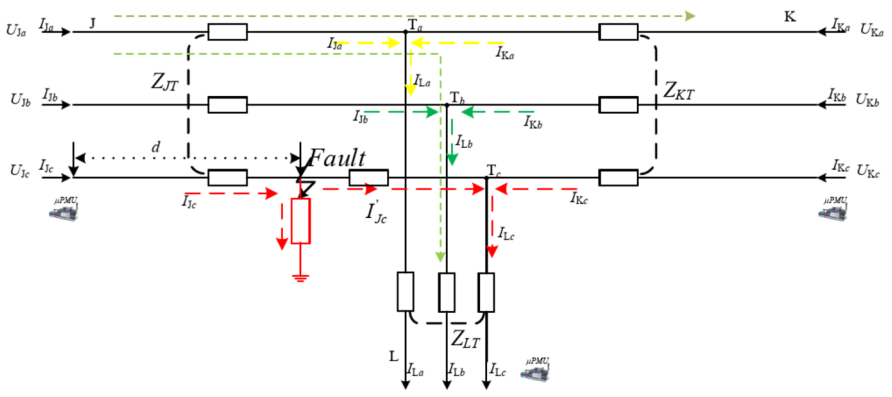

Fig. 6. Voltage and current analysis diagram for T-line fault operation.

$$
\begin{cases}
gg\,(1) = real\,(g\,(1)) = \begin{pmatrix} real\left(\dot{U}_{\mathrm{Ja}}\right) - D_{\mathrm{JT}} \times \begin{pmatrix} real(\dot{I}_{\mathrm{JTa}}) \times r_{\mathrm{JT-SI}} - imag\left(\dot{I}_{\mathrm{JTa}}\right) \\ \times 2\pi f \times l_{\mathrm{JT\text{-}SI}} + real(\dot{I}_{\mathrm{JTb}}) \times r_{\mathrm{JT\text{-}MI}} \\ - imag\left(\dot{I}_{\mathrm{JTb}}\right) \times 2\pi f \times l_{\mathrm{JT\text{-}MI}} + real(\dot{I}_{\mathrm{JTc}}) \\ \times r_{JT-\mathrm{MI}} - imag\left(\dot{I}_{\mathrm{JTc}}\right) \times 2\pi f \times l_{\mathrm{JT\text{-}MI}} \end{pmatrix} \\ - real\left(\dot{U}_{\mathrm{Ka}}\right) + D_{\mathrm{KT}} \times \begin{pmatrix} real(\dot{I}_{\mathrm{KTa}}) \times r_{\mathrm{KT\text{-}SI}} - imag\left(\dot{I}_{\mathrm{JTa}}\right) \\ \times 2\pi f \times l_{\mathrm{KT\text{-}SI}} + real(\dot{I}_{\mathrm{KTb}}) \times r_{\mathrm{KT\text{-}MI}} \\ - imag\left(\dot{I}_{\mathrm{KTb}}\right) \cdot 2\pi f \cdot l_{\mathrm{KT\text{-}MI}} + real(\dot{I}_{\mathrm{KTc}}) \cdot r_{\mathrm{KT\text{-}MI}} \\ - imag\left(\dot{I}_{\mathrm{KTc}}\right) \times 2\pi f \times l_{\mathrm{KT\text{-}MI}} \end{pmatrix} \end{pmatrix} \\
gg\,(1) = imag\,(g\,(1)) = \begin{pmatrix} imag\left(\dot{U}_{\mathrm{Ja}}\right) - D_{\mathrm{JT}} \times \begin{pmatrix} real(\dot{I}_{\mathrm{JTa}}) \times 2\pi f \times l_{\mathrm{JT\text{-}SI}} + imag\left(\dot{I}_{\mathrm{JTa}}\right) \\ \times r_{\mathrm{JT\text{-}SI}} + real(\dot{I}_{\mathrm{JTb}}) \times 2\pi f \times l_{\mathrm{JT\text{-}MI}} \\ - imag\left(\dot{I}_{\mathrm{JTb}}\right) \times r_{\mathrm{JT\text{-}MI}} + real(\dot{I}_{\mathrm{JTc}} \\ \times 2\pi f \times l_{\mathrm{JT\text{-}MI}} - imag\left(\dot{I}_{\mathrm{JTc}}\right) \times r_{\mathrm{JT\text{-}MI}} \end{pmatrix} \\ - imag\left(\dot{U}_{\mathrm{Ka}}\right) + D_{\mathrm{KT}} \times \begin{pmatrix} real(\dot{I}_{\mathrm{KTa}}) \times 2\pi f \times l_{\mathrm{KT\text{-}SI}} + imag\left(\dot{I}_{\mathrm{KTa}}\right) \\ \times r_{\mathrm{KT\text{-}SI}} + real(\dot{I}_{\mathrm{KTb}}) \times 2\pi f \times l_{\mathrm{KT\text{-}MI}} \\ + imag\left(\dot{I}_{\mathrm{KTb}}\right) \times r_{\mathrm{KT\text{-}MI}} + real(\dot{I}_{\mathrm{KTc}}) \\ \times 2\pi f \times l_{\mathrm{KT\text{-}MI}} + imag\left(\dot{I}_{\mathrm{KTc}}\right) \times r_{\mathrm{KT\text{-}MI}} \end{pmatrix} \end{pmatrix} \\
\vdots \qquad \vdots \qquad \vdots \\
gg\,(17) = real\,(g\,(9)) = \begin{pmatrix} real\left(\dot{U}_{\mathrm{Kc}}\right) - D_{\mathrm{KT}} \times \begin{pmatrix} real(\dot{I}_{\mathrm{KTc}}) \times r_{\mathrm{KT\text{-}SI}} - imag\left(\dot{I}_{\mathrm{KTc}}\right) \\ \times 2\pi f \times l_{\mathrm{KT\text{-}SI}} + real(\dot{I}_{\mathrm{KTa}}) \times r_{\mathrm{KT\text{-}MI}} \\ - imag\left(\dot{I}_{\mathrm{KTa}}\right) \times 2\pi f \times l_{\mathrm{KT\text{-}MI}} + real(\dot{I}_{\mathrm{KTb}}) \\ \times r_{\mathrm{JT\text{-}MI}} - imag\left(\dot{I}_{\mathrm{KTb}}\right) \times 2\pi f \times l_{\mathrm{KT\text{-}MI}} \end{pmatrix} \\ - real\left(\dot{U}_{\mathrm{Lc}}\right) + D_{\mathrm{LT}} \times \begin{pmatrix} real(\dot{I}_{\mathrm{LTc}}) \times r_{\mathrm{LT\text{-}SI}} - imag\left(\dot{I}_{\mathrm{LTc}}\right) \\ \times 2\pi f \times l_{\mathrm{LT\text{-}SI}} + real(\dot{I}_{\mathrm{LTa}}) \times r_{\mathrm{LT\text{-}MI}} \\ - imag\left(\dot{I}_{\mathrm{LTa}}\right) \times 2\pi f \times l_{\mathrm{LT\text{-}MI}} + real(\dot{I}_{\mathrm{LTb}}) \\ \times r_{\mathrm{LT\text{-}MI}} - imag\left(\dot{I}_{\mathrm{LTb}}\right) \times 2\pi f \times l_{\mathrm{LT\text{-}MI}} \end{pmatrix} \end{pmatrix} \\
gg\,(18) = imag\,(g\,(9)) = \begin{pmatrix} imag\left(\dot{U}_{\mathrm{Kc}}\right) - D_{\mathrm{JT}} \times \begin{pmatrix} real(\dot{I}_{\mathrm{KTc}}) \times 2\pi f \times l_{\mathrm{KT\text{-}SI}} + imag\left(\dot{I}_{\mathrm{KTc}}\right) \\ \times r_{\mathrm{KT\text{-}SI}} + real(\dot{I}_{\mathrm{KTa}}) \times 2\pi f \times l_{\mathrm{KT\text{-}MI}} \\ - imag\left(\dot{I}_{\mathrm{KTa}}\right) \times r_{\mathrm{KT\text{-}MI}} + real(\dot{I}_{\mathrm{KTb}}) \\ \times 2\pi f \times l_{\mathrm{KT\text{-}MI}} - imag\left(\dot{I}_{\mathrm{KTb}}\right) \times r_{\mathrm{KT\text{-}MI}} \end{pmatrix} \\ - imag\left(\dot{U}_{\mathrm{Kc}}\right) + D_{\mathrm{LT}} \times \begin{pmatrix} real(\dot{I}_{\mathrm{LTc}}) \times 2\pi f \times l_{\mathrm{LT\text{-}SI}} + imag\left(\dot{I}_{\mathrm{LTc}}\right) \\ \times r_{\mathrm{LT\text{-}SI}} + real(\dot{I}_{\mathrm{LTa}}) \times 2\pi f \times l_{\mathrm{LT\text{-}MI}} \\ + imag\left(\dot{I}_{\mathrm{LTa}}\right) \times r_{\mathrm{LT\text{-}MI}} + real(\dot{I}_{\mathrm{LTb}}) \\ \times 2\pi f \times l_{\mathrm{LT\text{-}MI}} + imag\left(\dot{I}_{\mathrm{LTb}}\right) \times r_{\mathrm{LT\text{-}MI}} \end{pmatrix} \end{pmatrix}
\end{cases} \tag{8}
$$

where r_{SI}, l_{SI}, r_{MI}, l_{MI} are the initial value of distribution line parameters, and f is real-time frequency values from the μPMU. The accuracy of the current μPMU's frequency estimation is greater than 1mHz, so the frequency provided by the μPMU can be assumed to be accurate[30].

In this way, the value ofξ, calculated for the 18 equations, can be used as a basis for the judgment of fault location initiation.

$$
\xi = \|gg\,(\cdot)\|_2 = \frac{1}{2} gg'\,(\cdot) \cdot gg\,(\cdot) \tag{9}
$$

Fault location algorithm design

When a fault occurs in a T-type line, the fault location has uncertainty, and it can appear at any location in the three interval segments of JT, KT, and LT. Establishing a localization model for the three segments is necessary when performing fault localization. Further analyzing Eq. (8), only 12 equations need to be established in each zone to estimate fault distance. The results of each zone are analyzed based on the discriminant method, and if the results meet the requirements, the fault distance and zone can be determined.

$$
\begin{cases}
h_{\mathrm{a}}(2) = \begin{pmatrix}
imag\left(\dot{U}_{i\mathrm{a}}\right) - d \times \begin{pmatrix} real(\dot{I}_{i\mathrm{Ta}}) \times 2\pi f \times l_{i\mathrm{T-SI}} + imag\left(\dot{I}_{i\mathrm{Ta}}\right) \\ \times r_{i\mathrm{T-SI}} + real(\dot{I}_{i\mathrm{Tb}}) \times 2\pi f \times l_{i\mathrm{T-MI}} \\ - imag\left(\dot{I}_{i\mathrm{Tb}}\right) \times r_{i\mathrm{T-MI}} + real(\dot{I}_{i\mathrm{Tc}}) \\ \times 2\pi f \times l_{i\mathrm{T-MI}} - imag\left(\dot{I}_{i\mathrm{Tc}}\right) \times r_{i\mathrm{T-MI}} \end{pmatrix} \\
- (D_{i\mathrm{T}} - d) \times \begin{pmatrix} real(\dot{I}_{q\mathrm{Ta}} - \dot{I}_{w\mathrm{Ta}}) \times 2\pi f \times l_{i\mathrm{T-SI}} + imag\left(\dot{I}_{q\mathrm{Ta}} - \dot{I}_{w\mathrm{Ta}}\right) \\ \times r_{\mathrm{JT-SI}} + real(\dot{I}_{q\mathrm{Tb}} - \dot{I}_{w\mathrm{Tb}}) \times 2\pi f \times l_{\mathrm{JT-MI}} \\ - imag(\dot{I}_{q\mathrm{Tb}} - \dot{I}_{w\mathrm{Tb}}) \times r_{i\mathrm{T-MI}} + real(\dot{I}_{q\mathrm{Tc}} - \dot{I}_{w\mathrm{Tc}}) \\ \times 2\pi f \times l_{i\mathrm{T-MI}} - imag(\dot{I}_{q\mathrm{Tc}} - \dot{I}_{w\mathrm{Tc}}) \times r_{i\mathrm{T-MI}} \end{pmatrix} \\
- imag\left(\dot{U}_{w\mathrm{a}}\right) + D_{w\mathrm{T}} \times \begin{pmatrix} real(\dot{I}_{w\mathrm{T}a}) \times 2\pi f \times l_{w\mathrm{T-SI}} + imag\left(\dot{I}_{w\mathrm{Ta}}\right) \\ \times r_{w\mathrm{T-SI}} + real(\dot{I}_{w\mathrm{Tb}}) \times 2\pi f \times l_{w\mathrm{T-MI}} \\ + imag\left(\dot{I}_{w\mathrm{Tb}}\right) \times r_{w\mathrm{T-MI}} + real(\dot{I}_{w\mathrm{Tc}}) \\ \times 2\pi f \times l_{w\mathrm{T-MI}} + imag\left(\dot{I}_{w\mathrm{Tc}}\right) \times r_{w\mathrm{T-MI}} \end{pmatrix}
\end{pmatrix} \\
h_{\mathrm{a}}(2) = \begin{pmatrix}
imag\left(\dot{U}_{i\mathrm{a}}\right) - d \times \begin{pmatrix} real(\dot{I}_{i\mathrm{Ta}}) \times 2\pi f \times l_{i\mathrm{T-SI}} + imag\left(\dot{I}_{i\mathrm{Ta}}\right) \\ \times r_{i\mathrm{T-SI}} + real(\dot{I}_{i\mathrm{Tb}}) \times 2\pi f \times l_{i\mathrm{T-MI}} \\ - imag\left(\dot{I}_{i\mathrm{Tb}}\right) \times r_{i\mathrm{T-MI}} + real(\dot{I}_{i\mathrm{Tc}}) \\ \times 2\pi f \times l_{i\mathrm{T-MI}} - imag\left(\dot{I}_{i\mathrm{Tc}}\right) \times r_{i\mathrm{T-MI}} \end{pmatrix} \\
- (D_{i\mathrm{T}} - d) \times \begin{pmatrix} real(\dot{I}_{q\mathrm{Ta}} - \dot{I}_{w\mathrm{Ta}}) \times 2\pi f \times l_{i\mathrm{T-SI}} + imag\left(\dot{I}_{q\mathrm{Ta}} - \dot{I}_{w\mathrm{Ta}}\right) \\ \times r_{\mathrm{JT-SI}} + real(\dot{I}_{q\mathrm{Tb}} - \dot{I}_{w\mathrm{Tb}}) \times 2\pi f \times l_{\mathrm{JT-MI}} \\ - imag(\dot{I}_{q\mathrm{Tb}} - \dot{I}_{w\mathrm{Tb}}) \times r_{i\mathrm{T-MI}} + real(\dot{I}_{q\mathrm{Tc}} - \dot{I}_{w\mathrm{Tc}}) \\ \times 2\pi f \times l_{i\mathrm{T-MI}} - imag(\dot{I}_{q\mathrm{Tc}} - \dot{I}_{w\mathrm{Tc}}) \times r_{i\mathrm{T-MI}} \end{pmatrix} \\
- imag\left(\dot{U}_{w\mathrm{a}}\right) + D_{w\mathrm{T}} \times \begin{pmatrix} real(\dot{I}_{w\mathrm{T}a}) \times 2\pi f \times l_{w\mathrm{T-SI}} + imag\left(\dot{I}_{w\mathrm{Ta}}\right) \\ \times r_{w\mathrm{T-SI}} + real(\dot{I}_{w\mathrm{Tb}}) \times 2\pi f \times l_{w\mathrm{T-MI}} \\ + imag\left(\dot{I}_{w\mathrm{Tb}}\right) \times r_{w\mathrm{T-MI}} + real(\dot{I}_{w\mathrm{Tc}}) \\ \times 2\pi f \times l_{w\mathrm{T-MI}} + imag\left(\dot{I}_{w\mathrm{Tc}}\right) \times r_{w\mathrm{T-MI}} \end{pmatrix}
\end{pmatrix}
\end{cases} \tag{10}
$$

where *i*, *q*, *w* represent the node numbers, and their respective ranges of values are J, K, L.

Referring to Eq. (10), the expressions for phase b and phase C can be written, and by combining the three sets of expressions a, b, and c, the fault location model of a zone can be composed. Based on Eqs. (4) and (6), the equations of faults in lines JT, KT, and LT can be constructed according to Eq. (10), respectively. Assuming that the fault is between KT, according to Eq. (4), only the equations of K-T-J, K-T-L two circuits need to be constructed, and according to Eqs. (10), 12 equation equations can be constructed, which is used as the solution model of fault localization. If the fault is between JT, construct the equations of the two circuits J-T-K, J-T-L, and 12 equivalent equations can be established. If the fault is between LT, construct the equations of L-T-K and L-T-J two circuits. According to Eqs. (10), 12 equations can be established.

$$
h(x) = \begin{cases}
h_a(1)\big|_{\text{K-T-J/J-T-K/L-T-K}} \\
h_a(2)\big|_{\text{K-T-J/J-T-K/L-T-K}} \\
h_b(1)\big|_{\text{K-T-J/J-T-K/L-T-K}} \\
h_b(2)\big|_{\text{K-T-J/J-T-K/L-T-K}} \\
h_c(1)\big|_{\text{K-T-J/J-T-K/L-T-K}} \\
h_c(2)\big|_{\text{K-T-J/J-T-K/L-T-K}} \\
h_a(1)\big|_{\text{K-T-L/J-T-L/L-T-J}} \\
h_a(2)\big|_{\text{K-T-L/J-T-L/L-T-J}} \\
h_b(1)\big|_{\text{K-T-L/J-T-L/L-T-J}} \\
h_b(2)\big|_{\text{K-T-L/J-T-L/L-T-J}} \\
h_c(1)\big|_{\text{K-T-L/J-T-L/L-T-J}} \\
h_c(2)\big|_{\text{K-T-L/J-T-L/L-T-J}}
\end{cases} \tag{11}
$$

Equation (11) then constitutes the fault localization model for the T-shaped line. In setting the unknown quantities, the line parameters are taken as unknown quantities: $r_{\text{JK-SI}}$, $l_{\text{JK-SI}}$, $r_{\text{JK-MI}}$, $l_{\text{JK-MI}}$, $r_{\text{LT-SI}}$, $l_{\text{LT-SI}}$, $r_{\text{LT-MI}}$, $l_{\text{LT-MI}}$, and the variables can be described as:

$$
x = \begin{bmatrix} D_{\mathrm{JT}} & d & r_{\text{JK-SI}} & l_{\text{JK-SI}} & r_{\text{JK-MI}} & l_{\text{JK-MI}} & r_{\text{LT-SI}} & l_{\text{LT-SI}} & r_{\text{LT-MI}} & l_{\text{LT-MI}} \end{bmatrix}' \tag{12}
$$

The solution of Eq. (11) is generally computed by numerical optimization. Trust-region(TR) is a better computational method for solving such equation[26]. However, it is necessary to solve the problem of the initial

radius of the trust-region method. In this paper, we use the Simulated Annealing Algorithm(SAA) to solve the approximate solution of the initial radius. The flow chart of the algorithm involved in this paper is shown:

```
# Algorithm 1 QNM
1. int Th=100℃,  T_min, S=0.01, K=0.9;
2. x0 =[5;0.5;0.05*ones(9,1)];
3. while Th>Tmin
4.              for j=1:11
5.                          dkt=doleg(g',g'', x (1));
6.                          x (1) = x (2:end)+dkt;
7.                          hkx = eval(g);
8.                          x_new(j)=x(j)+S*(S*MAX(j)*rand-MAX(j))

9.                          if  (x_new(j)>MIN(j))&&(x_new(j)<MAX(j)))
10.                                     dkt=doleg(g',g'', x_new(1));
11.                                     x_new(1) = x_new(2:end)+dkt;
12.                                     hkt = eval(g);
13.                                     delta = norm(hkt)-norm(hkx);
14.                                     if(norm(hkt)<norm(hxt))
15.                                                 x(j)=x_new(j);
16.                                     else
17.                                                 x(j)=x(j)
18.                                     end
19.                         end
20.                         Th=Th*K;
21.     end
22.end
```

Basis for determining the estimated results

In order to further constrain the results of the calculation, it is possible to further delimit the range of the parameter solution and set the upper limit of the line parameters after the introduction of the frequency, based on the conditions of determination in reference[25]. In the implementation of the algorithm in Fig. 7, the calculated results are local optimal solutions, not global optimal solutions. There will be some results that satisfy the evaluation conditions of reference[26], but the results are not the actual solution. Therefore, based on the analysis of a large number of line parameters, the upper limit can be statistically derived from the line manufacturer's data. In order to accurately determine whether the estimation result is the solution of the fault determination model, this paper further qualifies the determination conditions of the line parameters as shown in Eq. (13). By specifying Eq. (13), the calculation results are further restricted to reduce the probability of misjudgment.

$$\begin{cases} 0 < d < D \\ 0 < L_{\mathrm{JT}} < D \\ 0 < r_{\mathrm{SI}} < 0.5 \\ 0 < l_{\mathrm{SI}} < 0.05 \\ 0 < r_{SI} < 0.5 \\ 0 < l_{\mathrm{MI}} < 0.05 \end{cases} \tag{13}$$

where the value of D is taken as the lengths of the JT, KT, and LT lines.

Verification of experimental results

Data processing

Considering that the fault transient changes the line voltage and current in the initial phase of the fault will affect the micro-PMU estimation results. Therefore, after determining the fault moment based on Eq. (9) and waiting for 1–2 cycles, 20 sets of micro-PMU measurement data are selected for calculation. The procedure is shown in Fig. 8.

In the figure, t_0 is the moment of fault determination, and t_1 is the moment of fault localization model initiation. Since the action time of relay protection is not less than 50ms, the time interval between t_0 and t_1 should not be too long, generally 1–2 cycles can be taken.

In order to analyze the accuracy of the proposed method, the results can be processed and analyzed according to Eqs. (14)-(15).

$$\Delta = \left| x[\cdot]_{method} - x[\cdot]_{true} \right| \tag{14}$$

$$x_{\%} = \frac{\left| x[\cdot]_{method} - x[\cdot]_{true} \right|}{x[\cdot]_{true}} \times 100\% \tag{15}$$

Analysis of results

To verify the accuracy of the method proposed in this paper, a T-type line model is built in Matlab with the model parameters shown in Table 1. Different fault types and parameters are set, and a program is written in MATLAB to verify the algorithm.

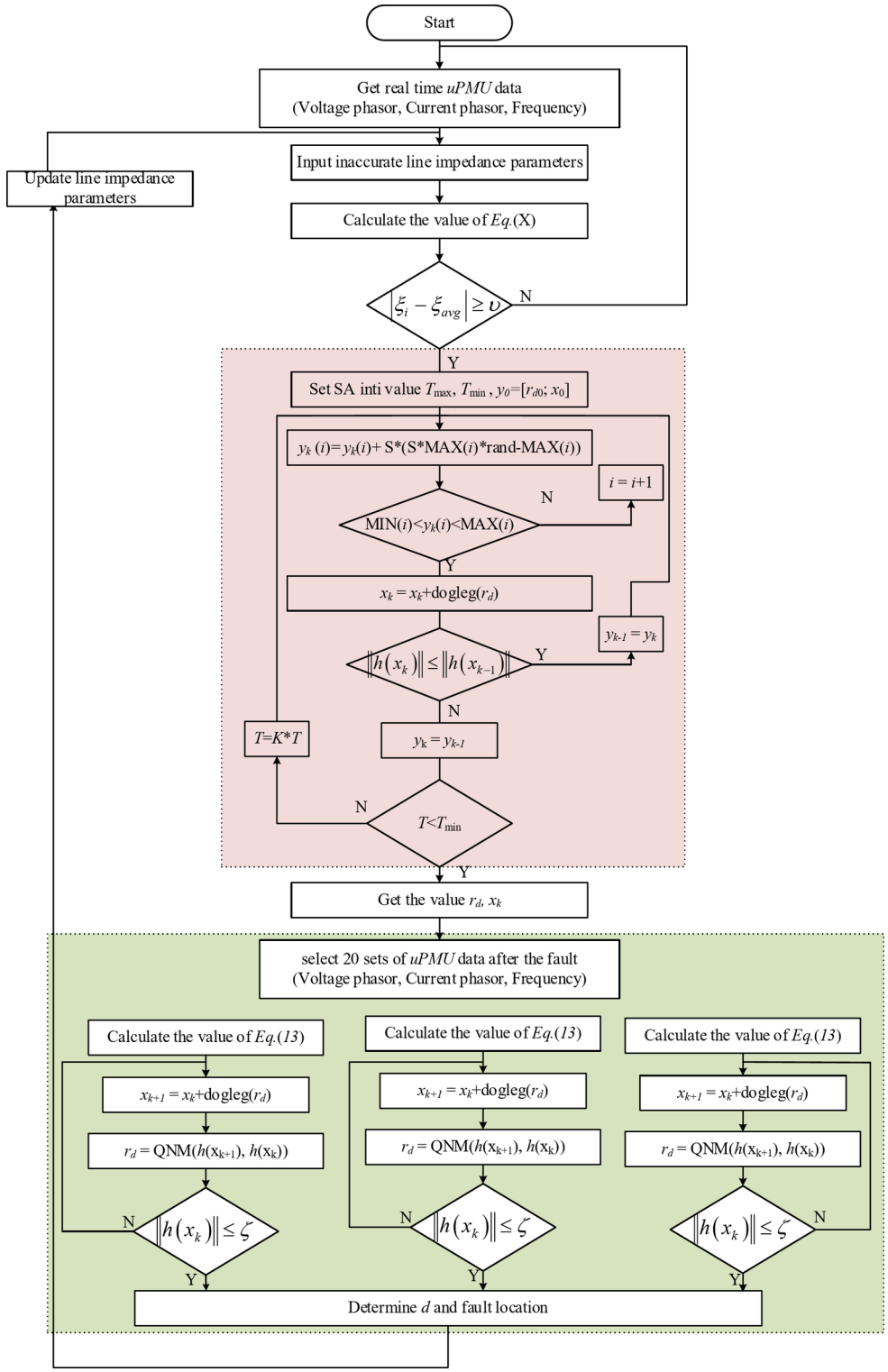

Fig. 7. SAA-TR algorithm flow chart.

Fault start time judge

To verify the accuracy of the fault determination moment method proposed in this paper, in the data in Table 1, build a T-type line model, set up a single-phase ground fault, a phase-seeing fault, and a fault resistance of 500Ω, respectively, at $t = 0.1$s. Calculate the voltage and current phase values corresponding to the fundamental wave and calculate the real-time deviation values. The results are shown in Fig. 9. Calculate the voltage and current phase values corresponding to the fundamental wave and calculate the real-time deviation values. The results are shown in Fig. 9:

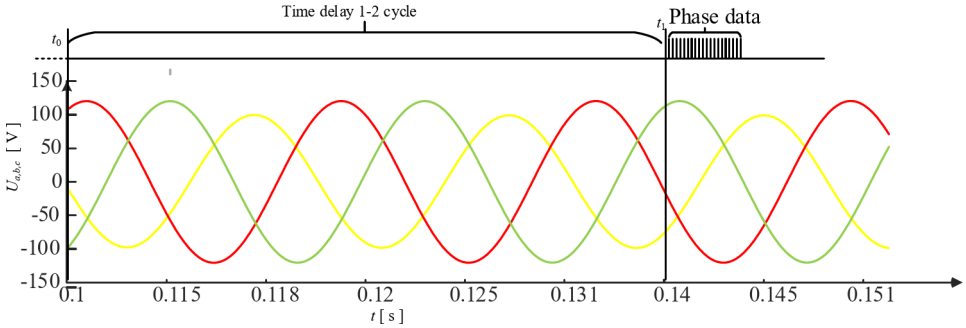

Fig. 8. Schematic diagram of data selection.

Line parameter	Value
Line JK self-resistance per length	0.2293 (Ω/km)
Line JK self-inductance per length	3.2252 (mH/km)
Line JK mutual-resistance per length	0.0353 (Ω/km)
Line JK mutual- inductance per length	1.4449 (mH/km)
Line LT self-resistance per length	0.382 (Ω/km)
Line LT self-inductance per length	2.3990 (mH/km)
Line LT mutual-resistance per length	0.05 (Ω/km)
Line LT mutual- inductance per length	1.0997 (mH/km)

Table 1. PI model line parameter.

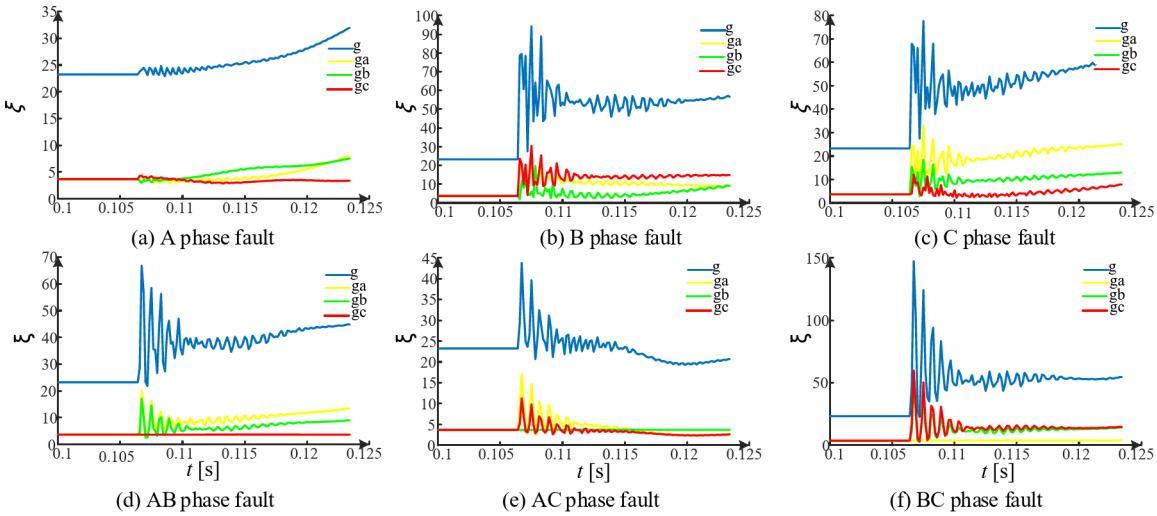

Fig. 9. Changes in g for different failure scenarios.

From Fig. 9, during normal operation, the deviation value of gg is basically unchanged, but if it is disturbed, its value will change according to the measured value. The figure shows that after $t = 0.1$s, the value of g fluctuates, which can be used as a time base for fault localization. After analyzing the changes of gg(a), gg(b), and gg(c) in different fault types, it can be seen that the residuals of a, b, and c corresponding to different fault types are different in each phase. Further analysis is needed to reflect the failure type by the residuals of each phase.

Error analysis of fault localization models

Applicable fault setting analysis

Generally, a fault resistance less than 100Ω is a low-resistance fault, and a fault greater than 100Ω is a high-resistance fault. Combined with the fault scenarios designed in reference[25,26], the method proposed in this paper is compared and analyzed in comparison with the applicability of the method proposed in the reference literature. An arc fault is constructed using the mentioned model in reference[26]. The results are shown in Table 2:

Method	Fault					
	< 100Ω	500Ω	1000Ω	1500Ω	2000Ω	Arc fault
This paper	Y	Y	Y	Y	Y	Y
[26]	Y	–	–	–	–	Y
[25]	Y	–	–	–	–	–

Table 2. Applicability analysis of different fault setting.

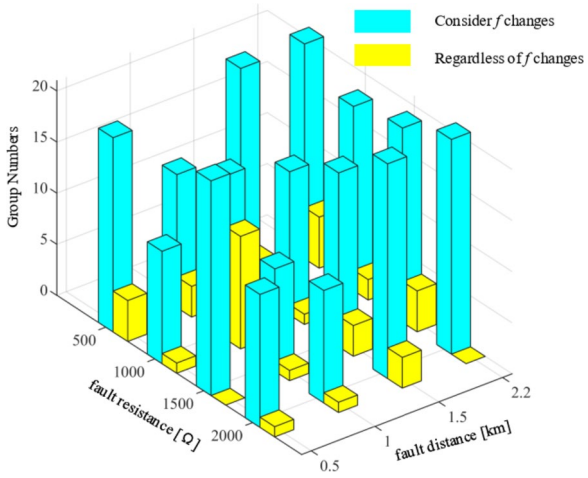

Fig. 10. Analysis of calculation results under different fault scenarios.

From Table 2, it can be seen that the method proposed in this paper has better applicability for fault scenarios and has some localization ability in high-resistance fault settings.

Effect of considering frequency and not considering frequency on localization results

Distribution network frequency has volatility, and its line impedance will change with the frequency value. The fault type and initial value are set to be consistent, and each of the 21 sets of phase data under different fault resistances and fault distances are selected for calculation and analysis to verify the influence of frequency parameters on the estimation process and results. The results are shown in Fig. 10:

As can be seen from Fig. 10, as the fault resistance increases, the localization model without the frequency has fewer values that satisfy the decision conditions in its 21 sets of calculation results. In contrast, the calculation results of the localization model designed in this paper that considers frequency are significantly higher than those of the localization model that does not consider frequency. In order to be able to verify the difference between the two localization models in terms of computational efficiency, the average number of iterations of the calculation results that meet the decision conditions under each error condition is calculated, and the results are shown in Fig. 11:

In the calculation process of the localization model, the calculation process involved in each iteration is the same, so the calculation time can be expressed by the number of iterations. As can be seen from Fig. 11 the number of computation iterations for the localization model proposed in this paper that takes frequency into account is significantly smaller than that for the localization model that does not take frequency into account. The reason for the lower number of computation iterations of the localization model without considering frequency is that it does not compute the value that satisfies the determination conditions in the test case of a faulted circuit of 1500Ω and a fault distance of 0.5 km.

Analysis of different fault localization results considering the effect of frequency

The distribution network frequency is not stable, its allowable fluctuations in the range of 2 Hz, and its line parameters will also change. The fault location model involved in this paper considers the effect of frequency variation on the estimation results of the fault location model. Set the frequency change range − 0.2 Hz–0.2 Hz, analyze the model without considering the frequency and consider the frequency in the calculation of efficiency and accuracy of the table laugh. The results are shown in Fig. 12.

From Fig. 12, it can be seen that by introducing frequency into the fault location model under the same fault setting conditions, the fault location model with frequency built in this paper requires much more computational time and computational accuracy than the fault location model without frequency.

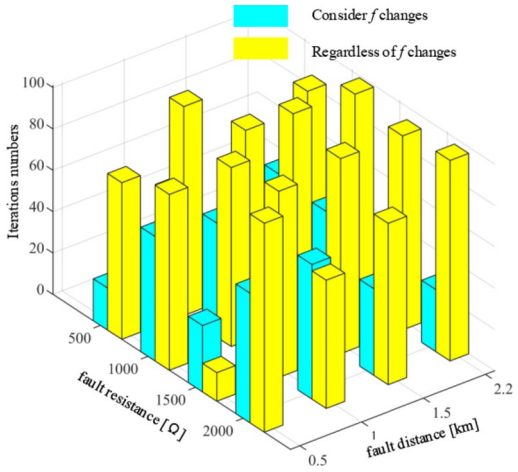

Fig. 11. Analysis of the number of iterations under different failure scenarios.

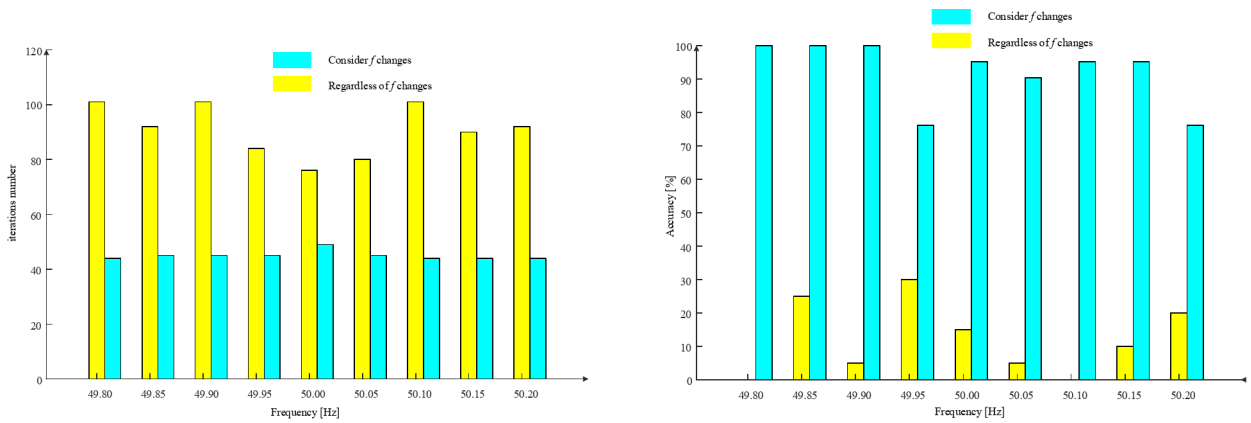

(a) Number of fault localization model calculations (b) Fault localization model estimation accuracy

Fig. 12. Effect of frequency variations on fault localization models under different fault scenarios.

Error analysis of estimated parameters of fault location models

The accuracy analysis of the estimation of fault distance and line parameters under different fault resistances and fault distances is analyzed to verify the accuracy of the fault location model established in this paper. The results are shown in Table 3.

From Table 3, it can be seen that the accuracy of fault distance under different fault conditions is much less than 100 m. Especially with the increase in fault distance, the fault model proposed in this paper can still meet the accurate estimation of fault distance. The data shows that the self-impedance estimation accuracy in the line parameters is higher than the mutual impedance parameter accuracy. In the analysis of fault distance accuracy, the parameters that affect its estimation accuracy are mainly line self-impedance parameters. If the fault distance accuracy requirement is not high, the influence of mutual impedance can be considered to be negligible.

Effect of different fault types on the estimation results of fault localization models

To verify the applicability of the fault location model established in this paper to different fault types, the line simulation models with different fault intervals, fault resistances, and fault distances are constructed, and their fault distances and line parameter estimation results are shown in Table 4:

As shown in Table 4, the fault location model proposed in this paper can still accurately locate the fault and estimate the fault distance for different fault intervals and fault resistance scenarios. The estimated fault distance is less affected by the actual fault distance and more affected by the fault resistance. As the fault resistance increases, the proposed model can still accurately estimate the fault distance, but the deviation of its line parameter estimation results will gradually increase.

Conclusion

This study introduced the frequency of operation of the distribution network into the parametric equations to construct a fault location model for three-terminal distribution lines. To address the sensitivity of the numerical

Parameter	Fault distance (m)	500Ω		1000Ω		1500Ω		2000Ω	
		Δ	%	Δ	%	Δ	%	Δ	%
d(m)	500	3.1574	0.6315%	0.7430	0.1486%	1.6805	0.3361%	10.6964	2.1393%
	1000	1.4192	0.1419%	2.3130	0.2313%	0.0007	0.0001%	0.0003	0.0000%
	1500	2.0837	0.1389%	0.9066	0.0604%	0.5909	0.0394%	2.0837	0.1389%
	2200	1.7639	0.0802%	0.2245	0.0102%	1.2004	0.0546%	1.7639	0.0802%
r_{SI} (Ω/km)	500	0.0005	0.2059%	0.0009	0.4077%	0.0007	0.3228%	0.0003	0.1429%
	1000	0.0009	0.4061%	0.0003	0.1148%	0.0007	0.2942%	0.0006	0.2751%
	1500	0.0002	0.0859%	0.0009	0.3710%	0.0005	0.2188%	0.0002	0.0859%
	2200	0.0000	0.0000%	0.0000	0.0000%	0.0000	0.0000%	0.0000	0.0000%
l_{SI} (mH/km)	500	0.0090	0.2786%	0.0044	0.1366%	0.0033	0.1012%	0.0205	0.6369%
	1000	0.0045	0.1409%	0.0096	0.2964%	0.0001	0.0030%	(0.0052)	0.1610%
	1500	0.0108	0.3354%	0.0091	0.2817%	0.0020	0.0609%	0.0108	0.3354%
	2200	0.0255	0.7894%	0.0010	0.0299%	0.0011	0.0345%	0.0255	0.7894%
r_{MI} (Ω/km)	500	0.0001	0.2816%	0.0005	1.4562%	0.0015	4.1942%	0.0004	1.1927%
	100	0.0006	1.7722%	0.0000	0.0426%	0.0014	3.9894%	0.0002	0.6128%
	1500	0.0000	0.0575%	0.0007	1.9897%	0.0010	2.8772%	0.0000	0.0575%
	2200	0.0011	2.9853%	0.0011	3.0098%	0.0012	3.2874%	0.0011	2.9853%
l_{MI} (mH/km)	500	0.0083	0.5729%	0.0038	0.2605%	0.0031	0.2162%	0.0195	1.3470%
	1000	0.0040	0.2748%	0.0090	0.6195%	0.0002	0.0114%	0.0048	0.3312%
	1500	0.0103	0.7126%	0.0085	0.5907%	0.0019	0.1344%	0.0103	0.7126%
	2200	0.0251	1.7345%	0.0013	0.0902%	0.0011	0.0752%	0.0251	1.7345%
r_{SI} (Ω/km)	500	0.0001	0.0183%	0.0002	0.0610%	0.0038	0.9890%	0.0003	0.0729%
	1000	0.0002	0.0573%	0.0004	0.0955%	0.0042	1.0868%	0.0000	0.0066%
	1500	0.0004	0.1140%	0.0074	1.9301%	0.0039	1.0306%	0.0004	0.1140%
	2200	0.0008	0.2218%	0.0013	0.3487%	0.0025	0.6533%	0.0008	0.2218%
l_{SI} (mH/km)	500	0.0196	0.8151%	0.0222	0.9252%	0.0321	1.3360%	0.0095	0.3978%
	1000	0.0211	0.8787%	0.0199	0.8298%	0.0351	1.4634%	0.0239	0.9960%
	1500	0.0187	0.7781%	0.0334	1.3923%	0.0461	1.9229%	0.0187	0.7781%
	2200	0.0079	0.3286%	0.0271	1.1281%	0.0339	1.4136%	0.0079	0.3286%
r_{MI} (Ω/km)	500	0.0008	1.5212%	0.0012	2.3290%	0.0012	2.4754%	0.0005	0.9054%
	1000	0.0009	1.7187%	0.0009	1.7083%	0.0014	2.7251%	0.0012	2.3553%
	1500	0.0007	1.4106%	0.0075	14.9932%	0.0020	3.9563%	0.0007	1.4106%
	2200	0.0009	1.8000%	0.0015	2.9147%	0.0013	2.5177%	(0.0009)	1.8000%
l_{MI} (mH/km)	500	0.0099	0.8958%	0.0085	0.7713%	0.0070	0.6364%	(0.0126)	1.1444%
	1000	0.0094	0.8560%	0.0098	0.8955%	0.0066	0.5990%	(0.0095)	0.8620%
	1500	0.0113	1.0259%	0.0042	0.3774%	0.0074	0.6688%	(0.0113)	1.0259%
	2200	0.0224	2.0328%	0.0041	0.3711%	0.0030	0.2740%	(0.0224)	2.0328%

Table 3. Parameter error analysis.

optimization solution to initial values, the simulated annealing algorithm was introduced to provide initial values for the fault location model, enhancing both the solvability and the accuracy of the estimation results.

1. By substituting the estimated values of voltage and current phasors into the operational process model, the fluctuation point of the residual values of the equations was determined. This point sets the time benchmark for initiating the fault location procedure and differentiating pre-fault and post-fault data.
2. The estimated frequency values were incorporated as parameters in the distribution line parameter model. Using these frequency values significantly improved the accuracy of the fault location model's estimation results, achieving accuracy more than three times higher than models that do not consider frequency. The fault distance estimation error was reduced to less than 50 m.
3. The confidence region demonstrated sensitivity to the initial radius when solving the problem. The confidence region and the simulated annealing approach were used to enhance further the fault location model's calculation process's solvability.

This work assumes that communication and time synchronization of end-node configured μPMUs functioning without issues, while more realistic scenarios should consider issues such as communication errors and time desynchronization. Future work will focus on analyzing the applicability of fault location methods for distribution networks under challenging conditions, including communication time asynchrony, as well as techniques to enhance location performance.

Fault section	Fault types	Fault resistance	d (m)	Δd (m)	z_{SI-JK}	z_{MI-JK}	z_{SI-LT}	z_{MI-LT}
JT	B-G	50	200	2.34	0.2294 + j1.0104	0.0350 + j0.4515	0.3812 + j0.7602	0.0503 + j0.3422
		100	500	5.12	0.2296 + j1.0088	0.0352 + j0.4502	0.3819 + j0.7586	0.0507 + j0.3419
		500	800	16.51	0.2317 + j1.0167	0.0369 + j0.4574	0.3826 + j0.7655	0.0522 + j0.3425
		1000	1000	1.83	0.2293 + j1.0120	0.0350 + j0.4522	0.3823 + j0.7615	0.0509 + j0.3429
		1500	1500	4.22	0.2356 + j1.0117	0.0414 + j0.4515	0.4040 + j0.4515	0.0723 + j0.3943
		2000	2200	4.70	0.2228 + j0.9969	0.0289 + j0.4383	0.3768 + j0.7495	0.0446 + j0.3344
KT	C-G	50	200	8.03	0.2286 + j1.0148	0.0342 + j0.4556	0.3782 + j0.7639	0.0476 + j0.3110
		100	500	8.20	0.2288 + j1.0152	0.0343 + j0.4562	0.3787 + j0.7635	0.0477 + j0.3435
		500	800	5.13	0.2286 + j1.0167	0.0343 + j0.4568	0.3803 + j0.7667	0.0490 + j0.3485
		1000	1000	5.92	0.2284 + j1.0167	0.0339 + j0.4565	0.3788 + j0.7655	0.0476 + j0.3445
		1500	1500	4.44	0.2314 + j1.0136	0.0372 + j0.4534	0.4435 + j0.7680	0.1112 + j0.3488
		2000	100	3.64	0.2318 + + 1.0331	0.0378 + j0.4745	0.3846 + j0.7775	0.0525 + j0.3604
LT	B-C	50	200	2.21	0.2282 + j1.0139	0.0339 + j0.4549	0.3799 + j0.7649	0.0491 + j0.3469
		100	500	2.15	0.2368 + j1.0249	0.0420 + j0.4659	0.3874 + j0.7727	0.0564 + j0.3542
		500	800	4.16	0.2300 + j1.0170	0.0355 + j0.4568	0.3811 + j0.7705	0.0499 + j0.3510
		1000	1000	2.38	0.2381 + j0.9966	0.0438 + j0.4377	0.3816 + j0.7533	0.0503 + j0.3350
		1500	1500	0.98	0.2305 + j1.0145	0.0363 + j0.4543	0.3582 + j0.7485	0.0266 + j0.3300
		2000	2200	10.58	0.2426 + j1.059	0.0484 + j0.4998	0.3965 + j0.7985	0.0065 + j0.3793
JT	A-B	50	200	3.99	0.2676 + j0.9473	0.0732 + j0.3937	0.3856 + j0.7284	0.0548 + j0.3102
		100	500	4.20	0.3938 + j0.8622	0.1993 + j0.3033	0.4468 + j0.6449	0.1159 + j0.2260
		500	800	5.88	0.2952 + j0.9526	0.1009 + j0.3925	0.3701 + j0.7614	0.0389 + j0.3425
		1000	1000	9.38	0.2323 + j1.0525	0.0377 + j0.4926	0.3775 + j0.7510	0.0467 + j0.3325
		1500	1500	2.98	0.2691 + j0.9781	0.0748 + j0.4182	0.3371 + j0.9040	0.0556 + j0.4848
		2000	2200	0.54	0.4645 + j1.1062	0.2429 + j0.4907	0.4736 + j0.8069	0.2422 + j0.3849
KT	A-C-G	50	200	5.45	0.2303 + j1.0142	0.0365 + j0.4540	0.3793 + j0.7350	0.0529 + j0.3410
		100	500	1.11	0.2279 + j1.0107	0.0348 + j0.4518	0.3769 + j0.7608	0.0504 + j0.3388
		500	800	5.93	0.2307 + j1.0164	0.0360 + j0.4559	0.3851 + j0.7652	0.0508 + j0.3442
		1000	1000	5.70	0.2307 + j1.01422	0.0361 + j0.4549	0.3828 + j0.7639	0.0518 + j0.3423
		1500	1500	4.94	0.2374 + j1.018	0.0429 + j0.4587	0.4040 + j0.8192	0.0728 + j0.3972
		2000	2200	0.21	0.2307 + j1.0135	0.0366 + j0.4647	0.3839 + j0.7627	0.0519 + j0.3445
LT	B-C-G	50	200	3.17	0.2288 + j1.0151	0.0345 + j0.4559	0.3803 + j0.7652	0.0492 + j0.3475
		100	500	2.12	0.2291 + j1.0148	0.0349 + j0.4559	0.3806 + j0.7652	0.0501 + j0.3475
		500	800	1.51	0.2286 + j1.0167	0.0343 + j0.4568	0.3804 + j0.7667	0.0490 + j0.3485
		1000	1000	2.77	0.2290 + j1.0158	0.0346 + j0.4568	0.3807 + j0.7662	0.0493 + j0.3454
		1500	1500	1.19	0.2296 + j1.0180	0.0354 + j0.4578	0.3789 + j0.7702	0.0473 + j0.3516
		2000	2200	2.43	0.2293 + j1.0157	0.0353 + j0.4568	0.3815 + j0.7662	0.0495 + j0.3485
JT	A-G	Arc fault	500	3.91	0.2162 + j0.9759	0.0323 + j0.4203	0.3707 + j0.7388	0.0452 + j0.3317
			1500	42.69	0.2194 + j0.9813	0.0331 + j0.4235	0.3720 + j0.7404	0.0462 + j0.3322
			2200	53.80	0.2264 + j0.9921	0.0342 + j0.4327	0.3467 + j0.7456	0.0479 + j0.3349

Table 4. Fault localization model estimation results for different fault scenarios.

Data availability

The original contributions presented in the study are included in the article/Supplementary Material. Further inquiries can be directed to the corresponding author.

Received: 15 July 2024; Accepted: 4 February 2025
Published online: 13 February 2025

References

1. Stefanidou-Voziki, P., Sapountzoglou, N., Raison, B. & Dominguez-Garcia, J. L. A review of Fault Location and classification methods in distribution grids. *Electr. Power Syst. Res.* **209**, 108031 (2022).
2. Furse, C. M., Kafal, M., Razzaghi, R. & Shin, Y. J. Fault diagnosis for electrical systems and power networks: a review. *IEEE Sens. J.* **21**, 888–906 (2021).
3. Ganivada, P. K. & Jena, P. A. Fault location identification technique for active distribution system. *IEEE Trans. Ind. Inf.* **18**, 3000–3010 (2022).
4. Panahi, H., Zamani, R., Sanaye-Pasand, M. & Mehrjerdi, H. Advances in transmission network fault location in modern power systems: review, outlook and future works. *IEEE Access.* **9**, 158599–158615 (2021).
5. Dashti, R., Daisy, M., Mirshekali, H., Shaker, H. R. & Hosseini Aliabadi, M. A survey of fault prediction and location methods in electrical energy distribution networks. *Measurement* **184**, 109947 (2021).

6. Li, Y., Zhang, M. & Chen, C. A deep-learning intelligent system incorporating data augmentation for short-term voltage stability assessment of power systems. *Appl. Energy*. **308**, 118347 (2022).
7. Deng, F., Li, X. & Zeng, X. Single-ended travelling Wave Protection Algorithm based on full waveform in the time and frequency domains. *IET Gener Transm Distrib.* **12**, 3680–3691 (2018).
8. Lopes, F. V. et al. Practical methodology for two-terminal traveling wave-based fault location eliminating the need for line parameters and time synchronization. *IEEE Trans. Power Deliv*. **34**, 2123–2134 (2019).
9. Lopes, F. V., Dantas, K. M., Silva, K. M. & Costa, F. B. Accurate two-terminal transmission line Fault Location using traveling waves. *IEEE Trans. Power Deliv*. **33**, 873–880 (2018).
10. Das, S., Santoso, S., Gaikwad, A. & Patel, M. Impedance-based Fault Location in Transmission Networks: theory and application. *IEEE Access.* **2**, 537–557 (2014).
11. Jia, K., Bi, T., Ren, Z., Thomas, D. W. P. & Sumner, M. High frequency impedance based Fault location in distribution system with DGs. *IEEE Trans. Smart Grid*. **9**, 807–816 (2018).
12. Pignati, M., Zanni, L., Romano, P., Cherkaoui, R. & Paolone, M. Fault Detection and Faulted Line identification in active distribution networks using synchrophasors-based real-time state estimation. *IEEE Trans. Power Deliv*. **32**, 381–392 (2017).
13. Zhang, Y., Wang, J. & Khodayar, M. E. Graph-based faulted line identification using micro-PMU data in distribution systems. *IEEE Trans. Smart Grid*. **11**, 3982–3992 (2020).
14. Livani, H. & Evrenosoglu, C. Y. A Fault classification and localization method for three-terminal circuits using machine learning. *IEEE Trans. Power Deliv*. **28**, 2282–2290 (2013).
15. Labrador Rivas, A. E. & Abrão, T. Faults in Smart Grid systems: monitoring, detection and classification. *Electr. Power Syst. Res.* **189**, 106602 (2020).
16. Ge, L., Li, Y., Li, Y., Yan, J. & Sun, Y. Smart distribution Network Situation Awareness for high-quality operation and maintenance: a brief review. *Energies* **15**, 828 (2022).
17. Jamali, S., Bahmanyar, A. & Bompard, E. Fault location method for distribution networks using smart meters. *Measurement* **102**, 150–157 (2017).
18. Von Meier, A., Stewart, E., McEachern, A., Andersen, M. & Mehrmanesh, L. Precision micro-synchrophasors for distribution systems: a summary of applications. *IEEE Trans. Smart Grid*. **8**, 2926–2936 (2017).
19. Sodin, D., Smolnikar, M., Rudež, U. & Čampa, A. Precise PMU-based localization and classification of short-circuit faults in power distribution systems. *IEEE Trans. Power Deliv*. **38**, 3262–3273 (2023).
20. Conte, F., D'Agostino, F., Gabriele, B., Schiapparelli, G. P. & Silvestro, F. Fault detection and localization in active distribution networks using optimally placed phasor measurements units. *IEEE Trans. Power Syst.* **38**, 714–727 (2023).
21. Ding, J., Wang, X., Zheng, Y. & Li, L. Distributed traveling-wave-based fault-location algorithm embedded in multiterminal transmission lines. *IEEE Trans. Power Deliv*. **33**, 3045–3054 (2018).
22. Li, Y., Cao, J., Xu, Y., Zhu, L. & Dong, Z. Y. Deep learning based on transformer architecture for power system short-term voltage stability assessment with class imbalance. *Renew. Sustain. Energy Rev.* **189**, 113913 (2024).
23. Yuan, J., Hu, Y., Liang, Y. & Jiao, Z. Faulty feeder detection for single line-to-ground fault in distribution networks with DGs based on correlation analysis and harmonics energy. *IEEE Trans. Power Deliv*. **38**, 1020–1029 (2023).
24. Lin, T. C., Lin, P. Y. & Liu, C. W. An algorithm for locating faults in three-terminal multisection nonhomogeneous transmission lines using synchrophasor measurements. *IEEE Trans. Smart Grid*. **5**, 38–50 (2014).
25. Wang Y. Parameter-free fault location algorithm for distribution network T-type transmission lines. *Energies* **12**, 1534 (2019).
26. Yun, Z., Wen, T. & Wang, C. Fault location method for three-terminal lines in distribution network based on line voltage measured by μMPMU. *IEEE Trans. Smart Grid*. **12**, 5095–5112 (2021).
27. Panahi, H., Sanaye-Pasand, M. & Davarpanah, M. Three-terminal lines fault location using two main terminals data in the presence of renewable energy sources. *IEEE Trans. Smart Grid*. **14**, 2085–2095 (2023).
28. Li, Y., Zhang, S., Li, Y., Cao, J. & Jia, S. PMU measurements-based short-term voltage stability assessment of power systems via deep transfer learning. *IEEE Trans. Instrum. Meas.* **72**, 2526111 (2023).
29. Abdelaziz, M. M. A., Farag, H. E., El-Saadany, E. F. & Mohamed, Y. A.-R. I. A novel and generalized three-phase power flow algorithm for islanded microgrids using a Newton trust region method. *IEEE Trans. Power Syst.* **28**, 190–201 (2013).
30. Belega, D., Fontanelli, D. & Petri, D. Dynamic phasor and frequency measurements by an improved Taylor weighted least squares algorithm. *IEEE Trans. Instrum. Meas.* **64**, 2165–2178 (2015).

Acknowledgements

We thank the National Natural Science Foundation of China (No. 52077028) for providing financial support for this study.

Author contributions

S.L. prepared the first draft of the manuscript; H.C. and C.W. supervised the research and revised the manuscript. X.S. and S.L. performed the experiments and analyzed the data. All authors have given approval to the final version of the manuscript.

Funding

This project is supported by the National Natural Science Foundation of China (No. 52077028).

Declarations

Competing interests

The authors declare no competing interests.

Additional information

Correspondence and requests for materials should be addressed to S.L.